Experimental and numerical study on seismic response of inclined tower legs of cable-stayed bridges during earthquakes

Jiang Yi[a,b], Jianzhong Li[a,*]

[a] State Key Laboratory of Disaster Reduction in Civil Engineering, Tongji University, 1239 Siping Road, Shanghai 200092, China
[b] Department of Civil Engineering, The University of Hong Kong, Pokfulam Road, Hong Kong, China

ABSTRACT

More than half of cable-stayed bridges adopt the tower with inclined legs, which can be loaded with a combination of bending, torsion, shear and axial force under earthquakes. To study the seismic response of inclined tower legs, shake table tests were conducted on a 1/20 scaled cable-stayed bridge model with an inverted Y-shaped tower. A description of the model design was introduced and observed damages including horizontal and diagonal cracks at inclined tower legs were presented. A numerical model, considering reduction of torsional stiffness of inclined tower legs after diagonal cracking, was established. The feasibility of the numerical model was validated by a comparison of numerical and test results, which showed good correlation in displacement response at tower top and deck end, and cable force. Based on numerical results, the crack torsional moment of the inclined tower could be easily reached at small peak ground acceleration (PGA), leading to a substantial reduction of torsional stiffness of the section. This reduction helped alleviate the torsional moment demand at larger PGAs and delay the torsional failure of the tower legs. Numerical results also revealed that the bending moment is the primary factor to cause concrete cracks at the lower regions of inclined tower legs whereas complex interaction of large bending moment and torsion results in flexural and torsional damage near the intersection. Conventional ways, which adopt an elastic behavior of torsion, either using stiffness prior to or after diagonal cracking, will lead to intensive overestimation or underestimation of torsional response of the inclined tower legs.

1. Introduction

In recent decades, with the continual development in design methodology and construction technology, cable-stayed bridges have gained worldwide popularity in spanning large distance, probably up to 1000 m. The ability of a cable-stayed bridge to span such large distance owes much to its supporting system: the decks are supported by cables that are diagonally resisted by strong stiff towers. Acting as the main load-bearing element, the tower is of critical importance to a cable-stayed bridge. In general, the tower should be designed to vertically resist large gravity load and also accommodate an amount of lateral loads associated with live loads, wind and seismic actions, and possible others [1].

The tower shape, by affecting load transmitting mechanisms, to some extent determines the success of a tower design. There are several tower shapes that have been successfully applied to practical engineering, namely H-shaped, A-shaped, inverted Y-shaped, single column, diamond-shaped and so forth. Fig. 1(a) shows the typical tower

configurations of cable-stayed bridges. A detailed analysis of the bridge tower shape inventory of 70 existing cable-stayed bridges in China shows that approximately 1/3 of cable-stayed bridges utilized H-shaped tower and another 1/3 adopted inverted Y-shaped tower while the rest occupied the remaining 1/3 [2], as shown in Fig. 1(b). Also note that more than half of the bridges utilized the tower with inclined legs (including Y-shaped, A shaped, and diamond-shaped). The preference of the tower with inclined legs owes to the aesthetical appearance, efficiency and stability of the structure.

However, the load condition of inclined tower legs can be extremely complicated during a longitudinal earthquake, as shown in Fig. 2. When longitudinal inertia force of the deck (V) is transmitted to tower top, it will result in bending moment $M_{y'}$ for a horizontal cross section (Section S′-S′ in Fig. 2), which in turn induces bending moment M_y and torsion T in the inclined cross section (Section S-S in Fig. 2). With gravity effects included, inclined tower legs can be loaded with a combination of bending, torsion, shear and axial force. Currently, for seismic design of towers, bending, shear and axial force are considered primary effects

---

* Corresponding author.
  E-mail address: lijianzh@tongji.edu.cn (J. Li).

Nomenclature

|	
A_0	area of the shear flow
A_e	total longitudinal reinforcement areas
A_t	transverse reinforcement area
A_g	gross area of member cross section
A_v	total cross sectional area of shear reinforcement
b	width of rectangular section
d	depth of section
d_1	effective depth of section in direction of loading
E_c	moduli of concrete
E_s	moduli of steel
F_x	friction force of sliding bearing
f_c	compressive stress of the concrete
f_w	confinement effective coefficient
f_{yh}	yield stress of stirrups
G	shear modulus of concrete
h	height of section
J_1	elastic torsional moment of inertia
J_2	post-cracking torsional moment of inertia
K_1	torsional stiffness before cracking
K_2	torsional stiffness after cracking
M_y	yield bending moment
M_{max}	maximum bending moment
N	normal compression force of the bearings
P	compressive force acting on section
p_0	perimeter of the shear flow
R_{Non}	response of nonlinear model
R_i	response of i model
s	stirrup spacing
t	thickness of tubular section
T_{cr}	cracking torsional moment
T_{max}	maximum torsional moment
T_y	yielding torsional moment
$\dot{u}_x$	relative velocity of bearings
V_c	concrete contribution to shear capacity
V_{max}	maximum shear force
V_n	shear capacity
V_s	reinforcement contribution to shear capacity
v_{tc}	nominal torsional shear stress
x_1	stirrup distance at short side of the section
y_1	distance of stirrup at long side of the section
β	discrepancy of maximum response
μ	sliding coefficient of friction
μ_ϕ	curvature ductility
μ_D	maximum local displacement ductility ratio
ϕ	peak curvature of a section
ϕ_y	yield curvature of a section
ν	Poisson ratio of concrete
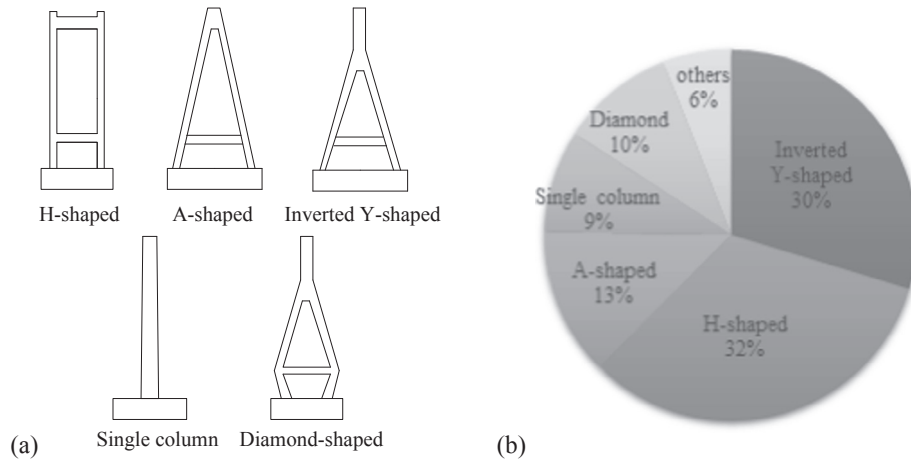
Fig. 1. Tower shapes of existing cable-stayed bridges in China: (a) tower shapes and (b) statistics.

[3–6], whereas torsion is limitedly recognized or valued. On the other hand, torsional moment can be significantly developed in irregular three-dimensional structures and torsional oscillations are often considered the cause of distress in buildings and bridges [7–9]. Consideration of torsion responses has been generally required in seismic design of these types of structures [10–13]. However, limited attention has been stressed on torsional behavior of inclined tower legs. To expand the knowledge on the behavior of cable-stayed bridge with inclined tower legs, it is essential that the effects of torsion be understood so that rational provisions can be made for design.

More importantly, cable-stayed bridges, usually with low damping ratios [14], are quite sensitive to large amplitude oscillations from earthquakes. The tower of cable-stayed bridges can develop significant nonlinear behavior or even suffer severe damage under strong earthquakes, as is the case of Ji-Lu cable-stayed bridge in Chi-Chi Earthquake [15] and Yokohama Bay Bridge in Great East Japan Earthquake [16]. For inclined tower legs subjected to large earthquake force, concrete crack is expected, either from flexural crack or torsional crack. Along with the occurrence of torsional cracks at tower legs, the torsional

stiffness of the tower decreases sharply [17,18]. It is revealed that the drop in torsional stiffness in pure torsion after cracking was generally much greater than the drop in flexural stiffness in pure bending [19]. The reduction of torsional stiffness will inevitably in turn influence the seismic response of the bridge. It is desirable to investigate the influence of reduction of torsional stiffness on seismic performance of cable-stayed bridges with inclined tower during an earthquake.

To address this problem, this paper illustrated shake table tests on a 1/20 scaled cable-stayed bridge model. Laboratory tests are used here to characterize the bridge in a more realistic way [20]. A description of the model design was presented and a numerical model which considered the reduction of torsional stiffness of inclined tower leg was established. The feasibility of numerical model was verified through a comparison of experimental and numerical results. An elaborate numerical analysis was conducted on seismic performance of inclined tower legs loaded with bending, torsion, shear and axial force. Further discussion was performed on different strategies to consider torsional stiffness of inclined tower leg and consequent seismic performance of the bridge. The object of this paper is to address the torsional effect on

seismic response of the cable-stayed bridge and shed light on further investigation of complex load condition of inclined tower legs.

2. Shake table tests

2.1. Prototype bridge

To investigate the torsional response of inclined tower legs of cable-stayed bridges, one typical bridge with an inverted Y-shaped tower is utilized as the prototype bridge. The inverted Y-shaped tower is selected here because 1/3 of cable stayed bridges adopted this type of tower (see Fig. 1), so as to account for the common cases. Fig. 3 shows the layout of the prototype bridge, which is a symmetric single tower cable-stayed bridge with two 230 spans, consisting of a concrete tower, double-plane cables, a steel deck and two concrete side piers.

The inverted Y-shaped tower is 150 m high from the bottom to the top and 60 m wide at the foundation level. It consists of two 106 m inclined tower legs, one 44 m anchor zone, and a 43 m rectangular crossbeam. Hollow rectangular boxes are used for inclined legs whose cross section gradually decreases from 14 m × 7.5 m at the foundation level to 8.5 m × 5 m at the intersection. The longitudinal steel ratio is approximately 2.17–2.51%.

The steel deck is formed into a streamlined closed box with welded flanges, webs, stiffeners and diaphragms. It has a width of 37.5 m and a height of 3.2 m high at middle span. The deck is supported by a total of 68 parallel wire cables and two side piers. The cables are diagonally arranged at anchor zone of the tower, forming into fan types. Two side piers are portal frames with a height of 34 m and a width of 25 m. The cross section of piers is 6.25 m × 5 m with the longitudinal steel ratio of 2.51%.

2.2. Test model design

The shake-table bridge model is designed as a 1:20 scaled geometric model of the prototype bridge, to fully exploit the dimensions and the payload capacity of the shaking table facilities. The geometrical characteristic of the test model is shown in Fig. 4.

In designing the inverted Y-shaped tower, micro-concrete was used with elastic modulus 1/3 of the prototype material. The cross section of inclined tower leg decreased from 0.66 m × 0.48 m at the foundation level to 0.4 m × 0.24 m at the intersection of two inclined legs and the thickness was 8 cm. Available rebar with a diameter of 6 mm and 3 mm in Chinese commercial market was used for longitudinal reinforcement and transverse reinforcement, respectively. The number and the

arrangement of longitudinal rebar were properly designed so that the towers and bent columns of the test model would have the same bending capacity exactly scaling down from the prototype bridge. The longitudinal steel ratio of tower sections is approximately 0.7–2.1%. The space of transverse rebar is set 3 cm, which is suitable for construction and also guarantees that bending failure appears prior to shear failure. The volumetric content of transverse reinforcement is approximately 0.2–0.5%. Besides, a strong beam was designed at the base of the tower to provide the fixed condition of the tower and also be used to move the tower onto and off the shake table.

Besides the tower, other components are also detailedly designed to satisfy the following two conditions – to provide a realistic representation of the prototype bridge response and to simplify construction of bridge model. The following actions are taken:

(1) For the deck, a regular box section composed of 10 mm thick steel plate was used to substitute the original streamlined steel box. The box section had exact scaling bending moment of inertia at both strong and weak axes from the prototype box.
(2) Original 68 cables of the prototype bridge were condensed to a total of 16 cables for the test model, following the principles of equivalent cable forces in the vertical direction and the dynamic characteristics from the prototype. High-strength stainless steel wires were used for the cables, each with a cross-sectional area of $7.85 \times 10^{-5} \, mm^2$.
(3) Sliding bearings were used to support the deck, which allowed movement in the longitudinal direction and prevented deformation in the transverse and vertical direction.
(4) For two side piers, solid section was used to substitute hollow section of the prototype. The cross section of piers was 0.3 m × 0.25 m with the longitudinal steel ratio of 0.5%.

Table 1 lists the material properties of the test model. Also note that in Fig. 4, the cables are numbered C1–C4 and some sections of inclined sections are named A-A, B-B, C-C, D-D and E-E, for later illustration. Fig. 5 depicts the shake-table test of the scale model.

2.3. Testing protocol

The input signal of the test was a near-field ground motion, TCU052 from the 1999 Chi-Chi Earthquake. Fig. 6 shows the acceleration, velocity and displacement time histories of the wave together with the acceleration spectrum. To account for the scale effect of the test model, the time axis of the prototype motion was compressed by 0.2236 (1/$\sqrt{20}$). The peak table acceleration was progressively increased during the test from 0.05 g to 0.7 g, at 0.05 g intervals, which yielded a total of 14 cases.

2.4. Observations

During the test, seismic damage was detected at the tower while the deck, cables and bents were visually undamaged. Fig. 7 shows the concrete cracks formed at inclined tower legs during the excitation. The concrete cracks first formed and extended at the bottom of inclined tower legs (Height = 0.25–0.7 m) at PGA = 0.3–0.5 g, as shown in Fig. 7(a). As PGA increased to 0.7 g, several horizontal parallel cracks formed at bottom region and middle region of the tower (Height = 0.7–2 m), as shown in Fig. 7(b), while cracks formed earlier remained almost unchanged. Meanwhile, horizontal and diagonal cracks together with slight concrete spalling appeared near the intersection of two inclined tower legs, as shown in Fig. 7(c). In Fig. 7(c), for better illustration, five sides of intersection are named Side A, B, C, D, E respectively. Concrete cracks were detected at Side A, Side C and Side E while no damage occurred at Side B and Side D. The cracks with red underlined were formed diagonally at Side A, Side E and Side C successively while other cracks were formed horizontally. Slight concrete
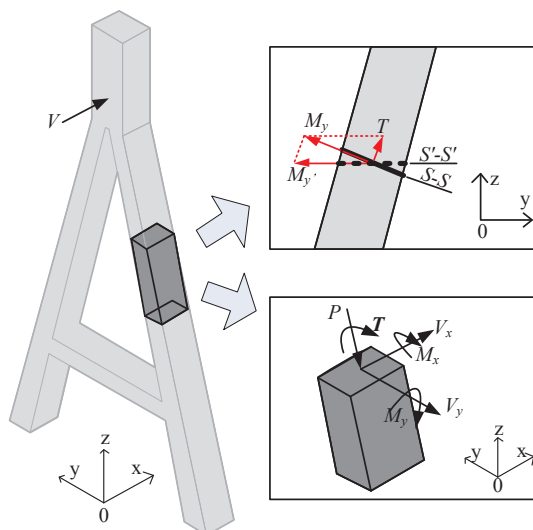

Fig. 2. Load condition of inclined tower leg under longitudinal earthquakes.

(a) General view of the bridge

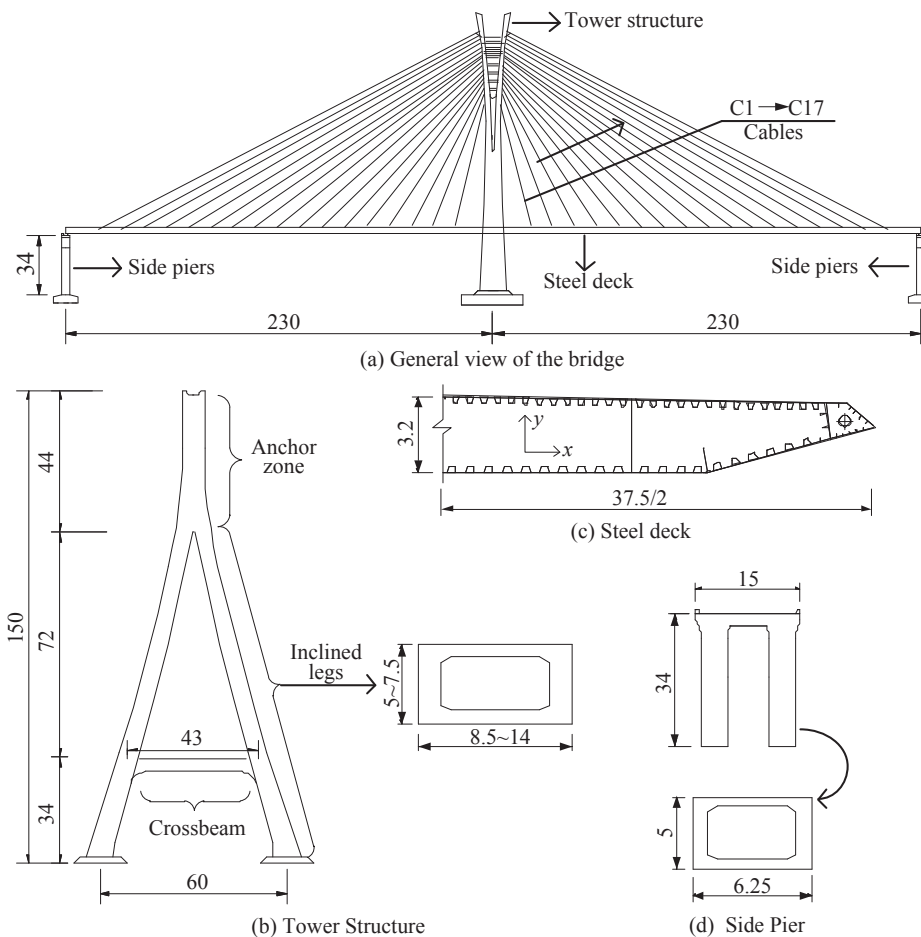(b) Tower Structure

(c) Steel deck

(d) Side Pier

Fig. 3. Description of the prototype bridge (Unit: m).

spalling also occurred at Side A and at the corner of Side C and Side E.

Even though obvious concrete cracks occurred at the tower legs, the test showed that the bridge system was stable during the test and had negligible residual displacement subjected to high amplitudes of excitations. In the test, larger PGAs (PGA = 0.75 g and PGA = 0.8 g) were sequentially applied to the bridge model, which at last failed at anchored zones of the tower with considerable concrete spalling and exposed longitudinal reinforcements. However, since analyzing the failure mode of the tower at anchored zones is beyond the scope of this study, it is not further discussed. More information can be found in Reference [21].

3. Numerical model

Due to large spans and the flexible cable-supporting system, cable-stayed bridges can quite easily develop nonlinear behavior during a seismic excitation. Both Nazmy [22] and Ren [5] recommended following nonlinear characteristics when modeling large long cable-stayed bridges for seismic analyses (1) sag effect of inclined cables, (2) combined axial load and bending moment interaction effect of towers and deck, (3) large displacement effect of the structure and (4) material nonlinearity. Besides the above nonlinearities, this study also considers nonlinear torsional response of tower legs. The background of torsional behavior of reinforced concrete (RC) members is first introduced here.

3.1. Background of torsional behavior of RC members

In three dimensions, the tower leg can be subjected to a total of six internal forces: three normal (axial force and two bending moments) and three tangential (torsion and two shear forces). In most of numerical models of the tower, bending, shear and axial behavior of RC members were included, while torsional behavior was seldom considered. To illustrate the behavior of the cable-stayed bridge during an earthquake, it is essential that the torsional property of tower leg be understood.

Laboratorial tests on RC hollow section members subjected to pure torsion up to failure can often lead to a typical T–θ curve, as shown in Fig. 8 [23]. This curve shows three different phases (Phase 1–3 of Fig. 8). Before the development of cracks (Phase 1), the torsional moment is resisted by concrete only, and torsional stiffness of RC beam can be considered to be constant K_1. The RC beam first cracks diagonally at T_{cr} when the principal tensile stress of concrete reaches its tensile strength. There is a sudden change in the local stiffness at and immediately adjacent to this first inclined crack. In the regions with inclined cracks, the torsional stiffness drops significantly, and space truss mechanism between concrete and stirrups is formed (Phase 2). Normally, it is feasible to assume 45° inclined concrete struts and linear behavior for the concrete and the steel [23]. At this stage, the slope of the torsional load-twist curve is K_2. When the stirrups first yield, the yielding torsional moment, T_y, is reached. After that, the truss mechanism will change due to nonlinear behavior of the materials and softening effect of the concrete [24] (Phase 3). At this stage, slightly larger torsion can be resisted by the RC members, but at the expense of large nonlinear response of the stirrups or concrete. The torsion failure is reached when either the strain of the concrete struts or the steel stain reaches the maximum value.

Since torsion failure of the RC members represents brittle shear-dominated failure, which may result in a fatal catastrophe of the
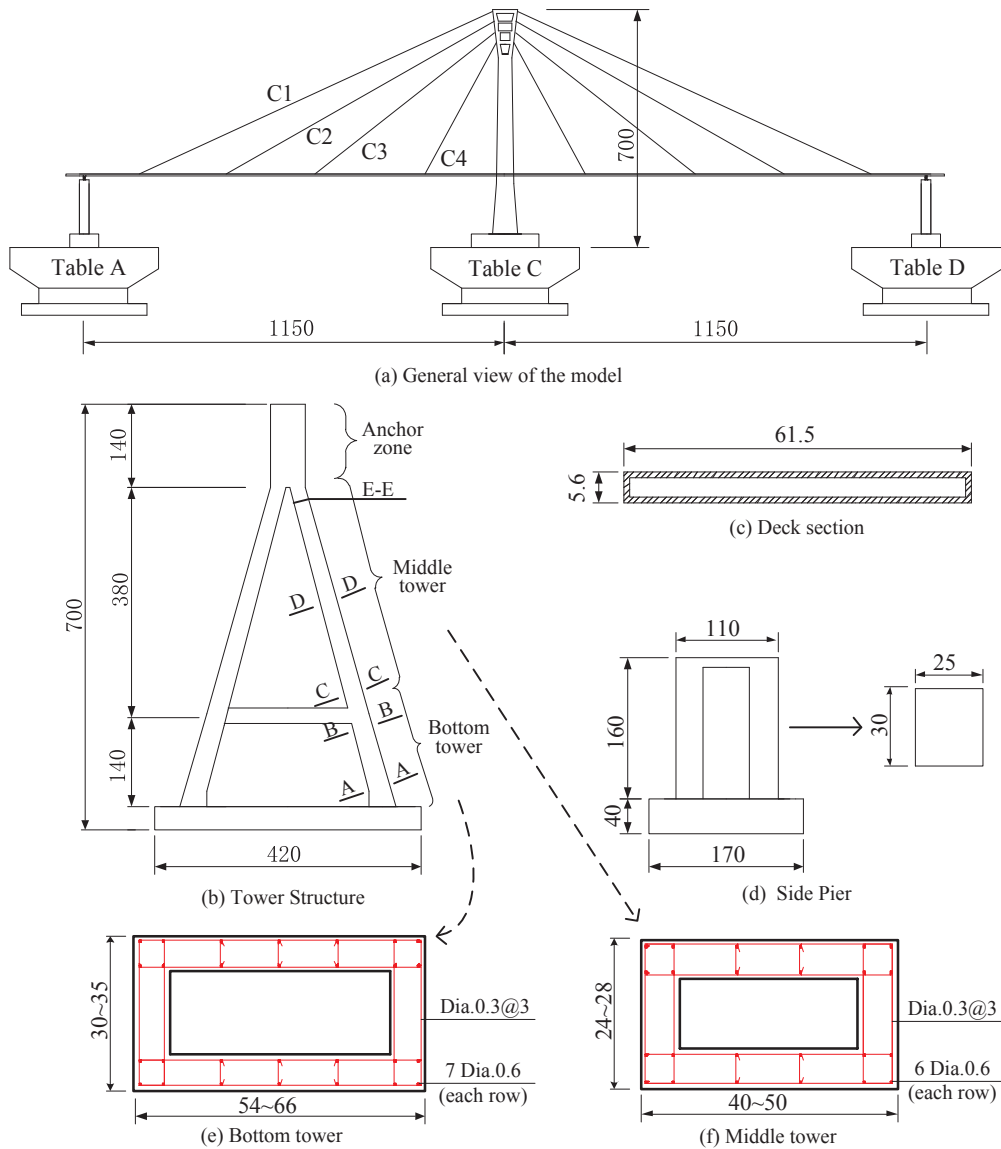
Fig. 4. Geometrical characteristics of test model (Unit: cm).

structure, this study only adopts Phase 1 and Phase 2, assuming torsion failure of the RC members was reached once yield torsion (T_y) was attended. The parameters that depict Fig. 8 are illustrated as follows.

3.1.1. Before cracking

Before cracking, the torsional moment is resisted by concrete only. The torsional moment of inertia J_1 can be determined via the elasticity method. For tubular section (which is the case of tower leg under study), J_1 is:

$$J_1 = \frac{4A_0^2 t}{p_0} = \frac{4[(h-t)(d-t)]^2 t}{2(h+d-2t)} \tag{1}$$

where A_0 and p_0 represent the area and perimeter of the shear flow in the tubular section (see Fig. 9(a)), and d is the width of the section; Thus the torsional stiffness before cracking is

$$K_1 = GJ_1 \tag{2}$$

where G is shear modulus of concrete, and $G = 1/[2 \times (1 + \nu)]$, where ν is the Poisson ratio; in this study and ν is assumed 0.2. In the presence of flexure, the cracking torsional moment is researched when [17]:

$$T_{cr} = \frac{d^2 h}{3} v_{tc} \tag{3}$$

where v_{tc} is the nominal torsional shear stress, and $v_{tc} = 0.2\sqrt{f_c}$, where f_c

Table 1
Material properties for the test model.

Material	Elastic modulus ($\times 10^3$ Mpa)	Compressive/yield stress (MPa)	Application
Micro-concrete	11.6	8.24	Concrete of Tower/side piers
6 mm rebar	200	400	Longitudinal reinforcement of Tower/side piers
3 mm rebar	200	400	Transverse reinforcement of Tower/side piers
Steel plate	200	235	Deck
Steel wires	195	1860	Cables

Fig. 5. Photo for full-bridge of the test model.

is the compressive stress of the concrete.

3.1.2. After cracking

Based on a space truss model, Lampert [19] revealed that post-cracking torsional stiffness can be regarded as independent of the shear force and also is not greatly influenced by bending. It can be represented by following function:

$$J_2 = \frac{4\bar{A}^2 E_s}{\bar{p} E_c} \sqrt{\frac{A_t A_e}{s\bar{p}}} \tag{4}$$

where E_S and E_C are the moduli for steel and concrete, $\bar{A}$ and $\bar{p}$ can be taken as 0.85 A_0 and 0.9 p_0 defined above; A_t and s are the transverse reinforcement area of a stirrup and the stirrup spacing, respectively; and A_e is the total longitudinal reinforcement areas. Thus the torsional stiffness after cracks is

$$K_2 = GJ_2 \tag{5}$$

The yielding torsional moment [17] is:

$$T_y = T_{cr} + \alpha_t \frac{x_1 \cdot y_1 \cdot A_t \cdot f_{yh}}{s} \quad \text{and} \quad \alpha_t = 0.66 + 0.33 * (y_1/x_1) \leqslant 1.50 \tag{6}$$

where x_1 and y_1 are the distance of stirrup at the short and long side of the section, as shown in Fig. 9(b), and f_{yh} is the yield strengthen of stirrups. The later part is the contribution of space truss which consists of stirrup tension members and diagonal concrete compression strut.

Table 2 shows the sectional torsion properties of inclined tower legs,

with section named in Fig. 3. Since the tower section reduces along with the tower height, J_1, J_2, T_{cr} and T_y gradually decreases from the bottom to the top. Meanwhile, with the onset of torsional cracks, the torsional stiffness of the section decreases sharply, with a reduction of approximately 94%.

3.2. Establishment of numerical model

In consideration of all sources of nonlinearities, a sophisticated model was conducted for the test model based on OpenSees framework [25].

3.2.1. Tower and bents model

The tower leg can be subjected to a combination of six internal forces during an earthquake. To consider bending, torsional, shear and axial behavior together, a section aggregator is used [26,27], as shown in Fig. 10. This command aggregates the following responses into a single section force-deformation model. (1) The axial-flexural response is described by means of fiber-section approach. This approach is established by discretizing the tower and bent section into unidirectional confined concrete, unconfined concrete and steel fibers. Both confined and unconfined concrete fibers were represented using the uniaxial Kent-Scott-Park model [28] with degraded linear unloading/reloading stiffness, whereas the steel fibers were represented using a bilinear hysteretic model with kinematic strain hardening. In this way, material nonlinearity and axial force-moment interaction effect was accounted for within the section. (2) Shear response is described by an elastic behavior; and (3) the torsion response is described by the bilinear law shown in Fig. 8. In this way, each Material-Object represents the section force deformation response for a particular degree-of-freedom. Then, flexibility-based elements with five Gauss-Lobatto integration points are employed. At each integration point, the section was applied by above section aggregator.

In the above modeling, the sectional interaction between torsion, shear and bending moment is ignored. This is because (1) for the concrete members with high span-to-depth ratio, the effect of shear stiffness on the total deflection is negligible [29], (2) under combined flexural displacement and torsional rotation, it's shown that plastic hinge capacity of columns is not affected adversely by torsional rotations up to 5% if well-distributed longitudinal reinforcement and stirrups are placed [30], and (3) torsion mechanics is not clearly understood and no contribution from longitudinal reinforcement was included in Eq. (6). On the other hand, axial-shear-bending-torsion interaction is achieved at the element level, where equilibrium is imposed and reached.
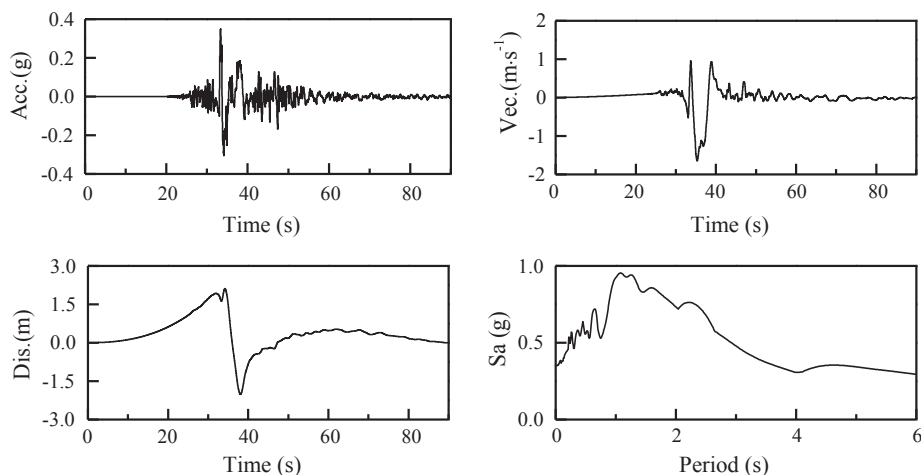

Fig. 6. Input ground motion histories and acceleration spectrum (5% damping).
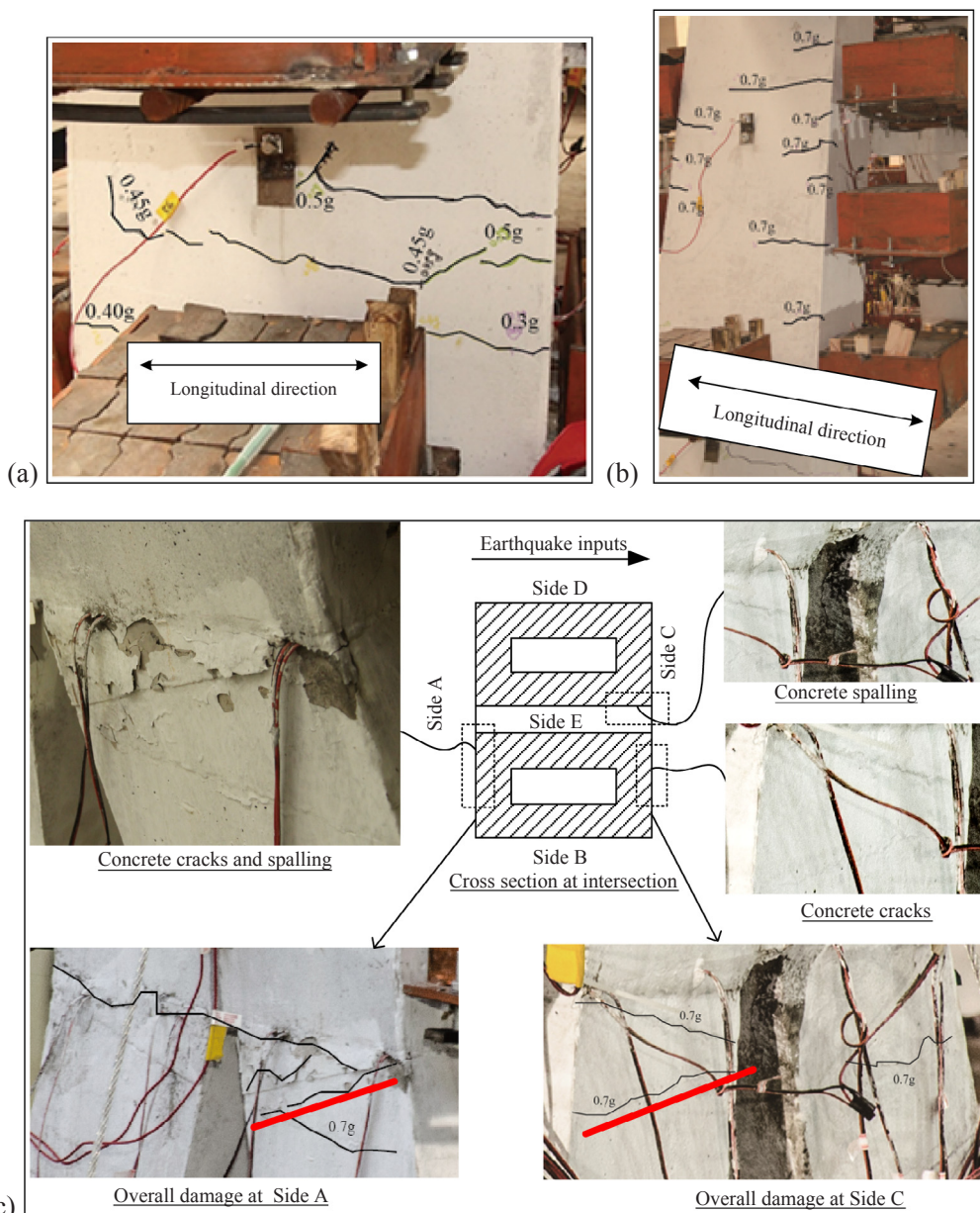
Fig. 7. Observed damage of inclined tower legs: (a) horizontal cracks at bottom tower (Height = 0.25–0.7 m); (b) horizontal cracks at middle tower (Height = 0.7–2 m); (c) horizontal and diagonal cracks with slight spalling near intersection (Height = 4.5–5 m).
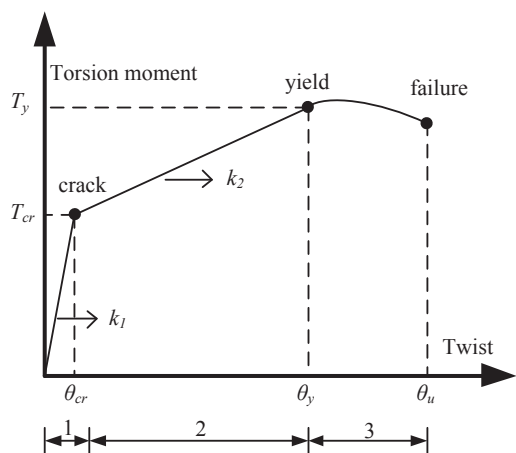

Fig. 8. Torsional twist-moment curve.

3.2.2. Modeling of other components

During the test, no damage occurred at the superstructure. The superstructure was modeled using linear-elastic element which can account for axial force-moment interaction and large displacement effect.

The stay cables were represented by truss elements, in which sag effect was accounted for using Ernst's equivalent elastic modulus concept [31]. Besides, initial strains were applied to cable materials so that the cable force resets at pre-stressed value under dead load.

The longitudinal behavior of sliding bearing was represented by friction models. The friction force was dependent on the normal compression force of the bearings N and sliding coefficient of friction μ, expressed as:

$$F_x = \begin{cases} -N \cdot \mu \cdot sng(\dot{u}_x) & N \leqslant 0 \\ 0 & N > 0 \end{cases} \tag{7}$$

where $\dot{u}_x$ depicts the relative velocity of bearings. Based on experimental results, the sliding coefficient of friction was a constant value of 0.15 [32]. In the transverse and vertical direction, the bearings were
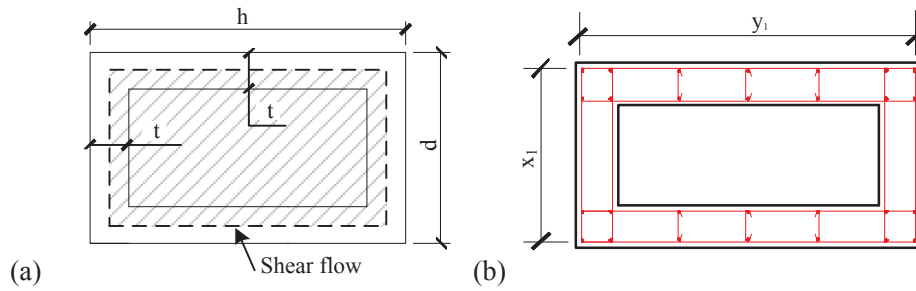
Fig. 9. Parameters of hollow sections: (a) shear flow and (b) distance of stirrup.

restrained.

3.2.3. Finite element model

Since the test model was fixed on the shake tables, the restraints of the supports in the numerical models were fixed. The finite element model is shown in Fig. 11. Before nonlinear seismic analysis, dead load was applied to the model prior to nonlinear dynamic analysis so that nonlinear seismic analysis starts from the equilibrium configuration of dead loads [5]. Rayleigh damping which incorporates 5% inherent damping was used based on 1st and 2rd longitudinal vibration period.

4. Measured and numerical results

4.1. Displacement response

To determine the adequacy of above numerical in estimating the seismic response of cable-stayed bridges, numerical and experimental results were compared. Achieved shake table motions was used to excite the numerical model. Some representative samples of the calculated and measured displacement histories at tower top and deck end are plotted in Fig. 12, and Table 3 lists the peak displacement of numerical and measured results for all the cases.

From Fig. 12, it can be seen that: (1) when PGA was small (PGA ≤ 0.4 g), although slight discrepancy existed between the numerical and measured time histories, numerical results caught the main features of the measured results for all the cases and the shapes of the time histories fitted in quite well, indicating close agreement of displacement response between numerical and measured results. (2) When PGA became large (PGA = 0.5–0.6 g), the discrepancy between numerical and measured results became obvious. This is mainly because the concrete cracks appeared at inclined tower legs in test model after PGA = 0.3–0.5 g, which altered the properties of the bridge model for the subsequent tests, whereas numerical model did not consider this damage accumulation. However, Table 3 reveals that for displacements at tower top and deck end, the maximum difference between numerical and measured results was less than 12% for all the cases, indicating a reasonable correlation between the numerical and measured results.

4.2. Cable response

Taken C3 as an example, Fig. 13 shows numerical and measured cable force histories. Similar to displacement response, when PGA was small (PGA ≤ 0.4 g), the shapes of the numerical and measured force

curves were alike for all the cases, showing good agreement of numerical and measured results. When PGA became larger (PGA > 0.4 g), the vitiation of calculated cable force was not as intense as measured results and the maximum cable force was slightly underestimated. However, the difference of peak response is less than 10%, which is acceptable for analytical modeling.

Based on the overall satisfactory correlation between the measured and calculated results, it was concluded that by modeling all sources of nonlinearities of the cable-stayed bridges including nonlinear torsion-twist behavior of inclined tower legs, numerical model can adequately simulate the response of the bridge during an earthquake.

5. Numerical study on seismic response of inclined tower legs

Since measured force response of inclined tower legs is not available, the response of inclined tower legs is studied numerically. The feasibility of numerical model is further assessed in comparison of structural damage predicted from numerical analysis and observed during the test. In this way, the numerical results serve to explain the observations of damage of inclined tower legs during the test and test results further verify the numerical results. The bending, torsional and shear response of inclined tower legs are illustrated respectively, as follows.

5.1. Bending

Normally, the curvature of a section is a good indicator of damage state of the section from bending. Based on the numerical model, normalized curvature response of inclined tower legs was presented in Fig. 14. The normalized curvature is expressed in the form of the curvature ductility:

$$\mu_\phi = \frac{\phi}{\phi_y} \tag{8}$$

where ϕ is the peak curvature of a section during earthquake and ϕ_y is the curvature when tensile reinforcement first yields. ϕ_y can be obtained either from empirical formulations or from cross section analysis. When $\mu_\phi < 1$, no reinforcement yields and the section is within elastic behavior, and as $\mu_\phi \geqslant 1$, the section develops material nonlinearity and bending cracks or concrete spalling is anticipated.

From Fig. 14, the sections near the cross beam were the most vulnerable region of the tower legs. These sections first reached yield curvature at PGA = 0.3 g, agreeing well with observed concrete cracks

Table 2
Sectional torsion properties of inclined tower legs.

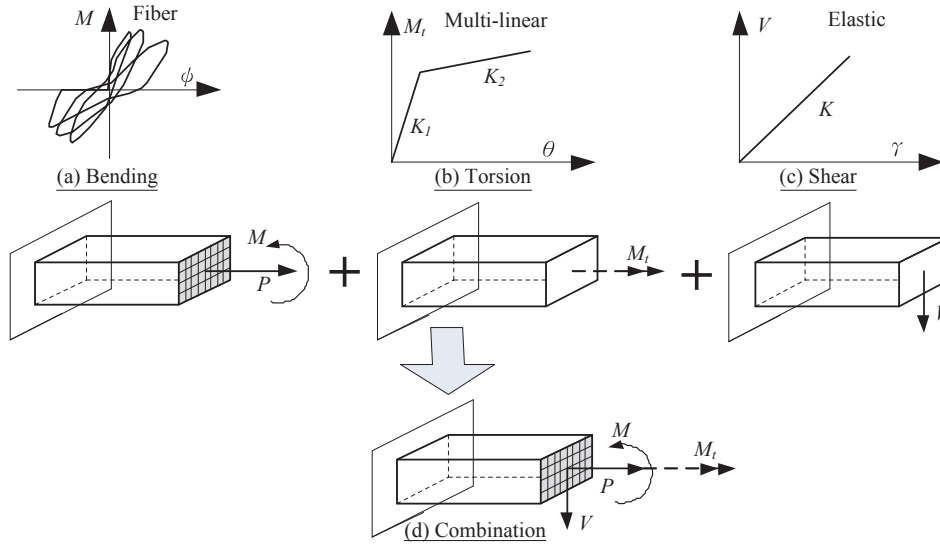| Section	J_1 ($\times 10^{-6}$ m^4)	J_2 ($\times 10^{-6}$ m^4)	J_2/J_1	T_{cr} (kN·m)	T_y (kN·m)	T_{cr}/T_y
A-A	4481	279	6.2%	15.1	43.6	34.7%
B-B	2637	170	6.4%	9.47	30.0	31.5%
C-C	2467	157	6.4%	8.84	28.2	31.3%
D-D	1636	111	6.8%	6.60	22.5	29.4%
E-E	894	73.4	8.2%	4.48	16.6	26.9%

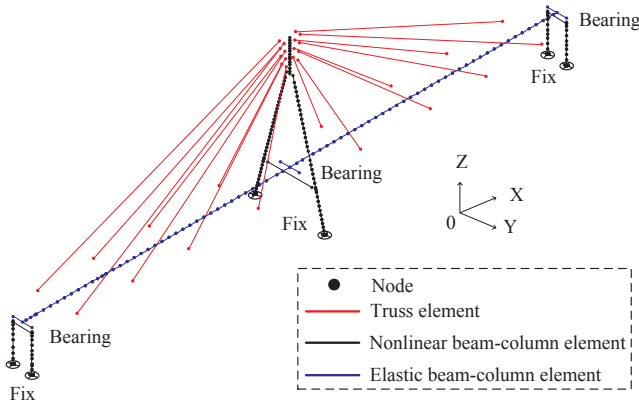Fig. 10. Section aggregate of inclined tower legs.

Fig. 11. Finite element model constructed in OpenSees.

in Fig. 7(a). As PGA increased, more sections reached yield limit. Unlike the pier of conventional girder bridges which for most cases had only one plastic region, the whole tower legs can be vulnerable to damage during the earthquake. This result fits in well with the observations during the test in Fig. 7(b). When PGA = 0.7 g, except for intersection, all other sections of inclined tower leg are beyond yield curvature. The maximum curvature ductility for PGA = 0.7 g is approximately 2.75 at the cross beam (Height = 1.5 m), which is considered as moderate damage [33]. This explains the observation during the tests that no obvious concrete spalling is observed at this region even when PGA is doubled after cracking.

5.2. Torsion

The torsion moment response of inclined tower leg is shown in Fig. 15, in which crack torsion moment (T_{cr}) and yield torsion moment (T_y) along the tower leg are also presented. Note that the crack moment and yield moment gradually decreased from the bottom of inclined tower leg to the top due to reducing dimension of the cross section.

Fig. 15(a), when PGA = 0.05 g, shows that the torsional moment of all sections is below the crack moment. Unlike crack moment, torsional moment remained almost the same along tower height. This led to crack torsional moment first exceeded at upper region of the tower legs (with tower height approximately from 4.5 m to 5 m when PGA was 0.1 g), while the rest part was within elastic range. The diagonal torsional cracks were anticipated at cracked regions, followed by a

reduction of torsional stiffness within this area. However, since these diagonal cracks were quite small and immediately closed after earthquake, no diagonal cracks could be visually observed at such PGAs during the tests. The cracking regions further expanded to lower heightwith the increase of PGAs. When PGA sequentially increased to 0.35 g, except for bottom region of the tower (with tower height around 0–1 m), torsional moment of all sections almost reached or exceeded crack moment, indicating a further reduction of tower torsional stiffness. When PGA further increased to 0.5–0.7 g, crack moment was almost exceeded for all sections. Also note from Fig. 15 that after reaching crack torsional moment, torsion moment continued to increase with PGAs, but was smaller than yield torsional moment for all the cases.

5.3. Shear force

To better illustrate the shear response of inclined tower legs, the shear force is normalized by nominal shear force capacity (V_n), which for a hollow section is calculated as [34]:

$$V_n = V_c + V_s \tag{9a}$$

$$V_c = 0.0256\alpha'\left(1 + \frac{P}{2A_g}\right)\sqrt{f_c}A_g \tag{9b}$$

$$V_s = \frac{A_t \cdot f_{yh} \cdot d_1}{s} \tag{9c}$$

$$0.3 \leqslant \alpha' = \frac{f_w}{0.15} + 3.67 - \mu_D \leqslant 3 \tag{9d}$$

$$f_w = 2\rho_w f_{yh} \leqslant 0.35 \tag{9e}$$

$$\rho_w = \frac{A_v}{bs} \tag{9f}$$

where V_c and V_s are concrete contribution and reinforcing steel contribution to shear capacity, respectively; P is the compressive force acting on section; A_g is gross area of member cross section, d_1 is the effective depth of section in direction of loading measured from the compression face of the member to the center of gravity of the tension reinforcement; μ_D is the maximum local displacement ductility ratio of member; A_v is total cross sectional area of shear reinforcing bars in the direction of loading; b is the width of rectangular column.

Fig. 16 shows the normalized shear force of inclined tower leg along tower height. One can see that shear force gradually increased with the
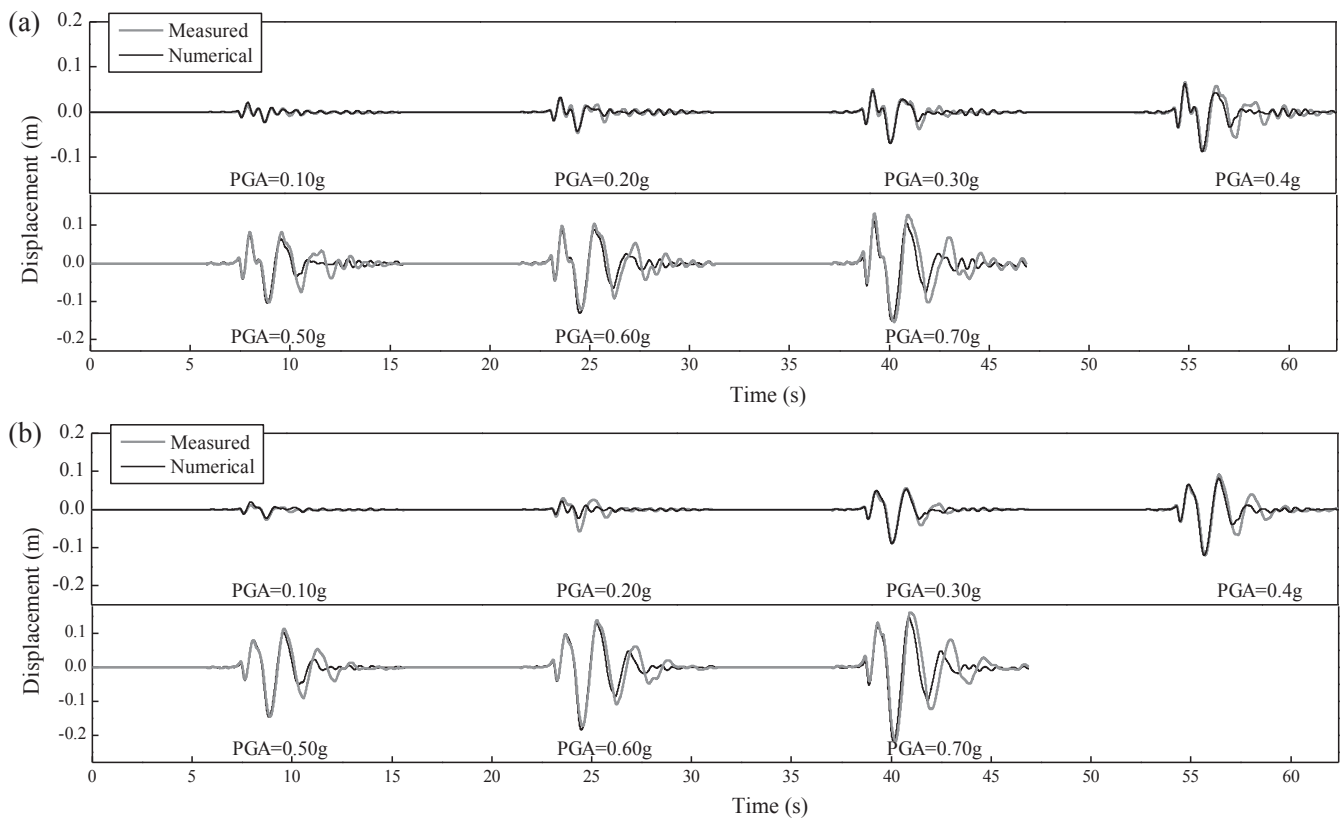
Fig. 12. Comparison of numerical and measured time history of displacement at: (a) tower top and (b) deck end.

Table 3
Comparison of numerical and measured peak displacements.

PGA (g)	Tower displacement (mm)			Deck displacement (mm)		
	Measured	Numerical	Error	Measured	Numerical	Error
0.05	8.2	9.0	8.9%	8.5	8.6	1.6%
0.10	22.8	24.3	6.5%	26.1	24.6	−5.9%
0.15	35.0	36.0	2.9%	41.3	42.6	3.1%
0.20	46.5	42.0	−9.7%	56.8	53.1	−6.6%
0.25	57.6	58.1	0.9%	73.7	73.9	0.2%
0.30	67.9	69.1	1.8%	91.7	89.4	−2.5%
0.35	78.7	80.4	2.1%	113	106.4	−6.0%
0.40	86.5	89.7	3.8%	127	120.7	−4.9%
0.45	93.7	98.4	5.1%	140	133.7	−4.7%
0.50	102	106	3.7%	155	145.5	−6.0%
0.55	111	113	1.7%	170	157.2	−7.4%
0.60	121	124	2.3%	187	176.0	−6.0%
0.65	132	134	1.7%	204	192	−6.1%
0.70	154	150	−2.8%	239	218	−9.1%

PGAs, despite flexural cracks appeared after PGA = 0.3 g. For all PGAs, the normalized shear force is less than 0.2, showing that shear alone would far less lead to diagonal cracks during the earthquake.

5.4. Prediction of damage zones

Loaded with a combination of bending moments, torsional moments, shear forces, and axial force, it is difficult to assess stress distribution of inclined tower legs, especially when the tower goes into inelastic range. Based on available literatures regarding a combination of bending, torsion, shear and axial force, some conclusions can be drawn as follows:

(1) There is limited interaction between bending moment and torsion for reinforced concrete specimens until either or both the bending moment and torque exceeded 50 percent of the strength of the specimen in pure bending and pure torsion respectively [35].

(2) There was a significant interaction between torsion and shear since both of them cause inclined tensile stresses [35].

(3) At a low level of axial compression, the torsional capacity of columns is slightly enhanced, and square columns exhibited localized torsional damage [36].

(4) The shear capacity of the columns under bending and shear increased with reduction in aspect ratio, but both the displacement and twist at ultimate shear and ultimate torque of the columns under combined loadings reduced significantly [7].

(5) Despite some numerical models or experiments [37–41] has been published concerning the behavior of specimens subjected to axial force, torsion, shear and bending, none of them are applicable to estimate onset of the damage of concrete sections.

Based on above conclusions, two criteria are adopted to determine structural damage of inclined tower legs. The first criterion considered the interaction of torsion and moment as [42]:

$$\left(\frac{T}{T_y}\right)^2 = r\left(1 - \frac{M}{M_y}\right) \tag{10}$$

where T and M are applied torque and bending moment, respectively; T_y and M_y are the yield torque and bending moment, respectively; and r is the ratio of yield force of flexure tension and compression reinforcement; for a symmetric section, $r = 1$.

Another criterion involved interaction of torsion and shear, as [43]:

$$\left(\frac{T}{T_y}\right)^2 + \left(\frac{V}{V_n}\right)^2 = 1 \tag{11}$$

where V and V_n are applied shear force and nominal shear force capacity.

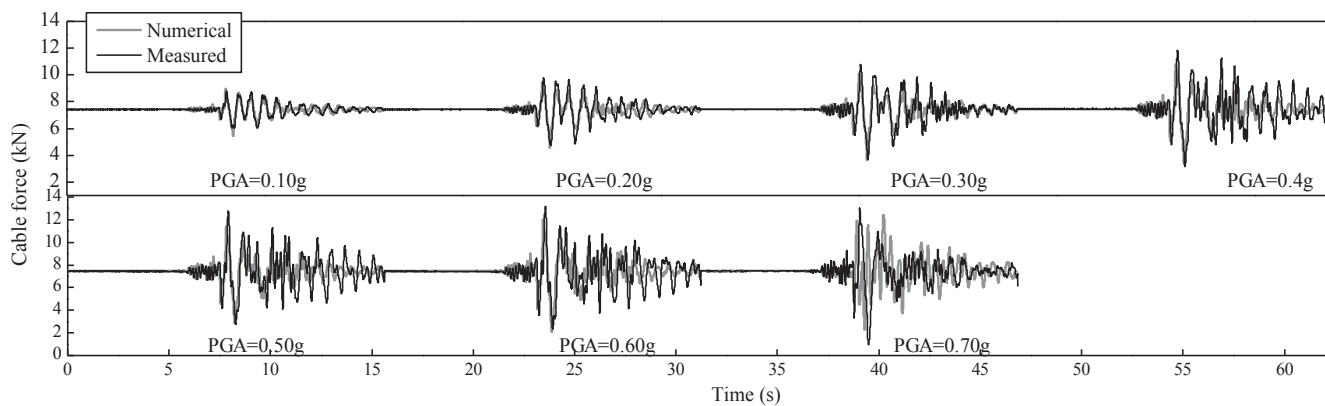Based on Eqs. (10) and (11), two structural damage limit are defined

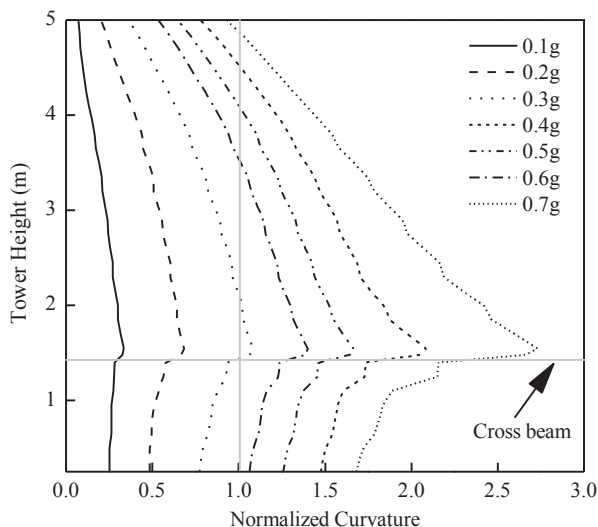**Fig. 13.** Comparison of numerical and measured time history of cable force (C3).

Fig. 14. Normalized curvature of inclined tower legs along tower height.

as follows:

$$C_{tb} = \left(\frac{T_{max}}{T_y}\right)^2 + \left(\frac{M_{max}}{M_y}\right) \tag{12a}$$

$$C_{tv} = \left(\frac{T_{max}}{T_y}\right)^2 + \left(\frac{V_{max}}{V_n}\right)^2 \tag{12b}$$

where T_{max}, M_{max} and V_{max} are the maximum torsional moment, maximum bending moment and maximum shear force during the earthquake, respectively. In this way, C_{tb} and C_{tv} refers to damage limit from interaction of torsion and bending, and from torsion and shear, respectively. When $C_{tb} < 1$, there would be no cracks from interaction of torsion and moment while $C_{tb} \geqslant 1$ indicates possible structural damage (either horizontal and diagonal concrete permanent cracks or steel yielding) from torsion and moment. Similar to C_{tb}, $C_{tv} \geqslant 1$ refers to potential structural damage from torsion and shear. However, since Eqs. (10) and (11) were developed conservatively for section design, neither $C_{tb} \geqslant 1$ or $C_{tv} \geqslant 1$ would ascertain structural damage at the section, but indicated the applied forces were beyond the design limit.

Fig. 17 shows the C_{tb} and C_{tv} along tower height for different PGAs. When PGA = 0.3 g, C_{tb} first reached design limit at the regions above the crossbeam, indicating possible structural damage first occurred at this region. After PGA > 0.3 g, C_{tb} further increased and was larger than 1 for all sections when PGA $\geqslant$ 0.5 g. On the other hand, C_{tv} was less than 1 for all the cases, showing no structural damage from the interaction of torsion and shear. The most vulnerable part to torsional and

shear damage is located at the regions near the intersection. Thus, it can be concluded that the structural damage observed during the test mainly came from interaction of torsion and bending.

Fig. 18 further illustrates the relative contribution of torsion, bending and shear to C_{tb} and C_{tv} at PGA = 0.7 g. From Fig. 18(a), for lower inclined tower (Height = 0–4 m), bending made the most contribution (larger than 80%) to C_{tb} while the contribution from torsion could be neglected. This explains the observations during the test that bending cracks dominated at the bottom and middle tower. However, for the upper inclined tower (Height = 4–5 m), the contribution from torsion increased to a much larger extent (larger than 20%). Especially at intersection, torsion occupied approximately 40% to the total value of C_{tb} so that torsional effect cannot be ignored. Under a combination of large torsion and bending, and also possible stress concentration, the region near intersection experienced both bending cracks and torsional cracks, as shown in Fig. 7(c). From Fig. 18(b), torsion made the most contribution to C_{tv} (larger than 85% for all the sections), while the contribution of shear was of no significance. Above results indicate that bending moments were the primary factor that caused concrete cracks at bottom of the tower, and the complex interaction of large bending moment and torsion led to flexure and torsional damage near the intersection, whereas shear force made negligible contribution to the damage of inclined tower legs.

6. Influence of torsional stiffness

This section further investigates the influence of different torsional stiffness choice on predication of seismic response of the bridge. Normally, when modeling tower structures, a constant torsional stiffness was applied to inclined tower legs since reduction of tower torsional stiffness during the earthquake is seldom recognized or valued. To reveal the influence of torsional stiffness choice, two more models in addition to the above numerical model (referred to Nonlinear model later) were established, namely Elastic model and Crack model. These two models are identical to the Nonlinear model (including bending and shear modeling) except that an elastic behavior was applied to the torsional stiffness of inclined tower legs: Elastic model: $K_e = K_1$, and Crack model: $K_c = K_2$. Thus, Elastic model referred to the normal case which only considered elastic behavior at Phase 1 (see Fig. 8), neglecting the reduction of torsional stiffness, while Crack model referred to the case which only adopted crack stiffness of Phase 2, neglecting the elastic behavior at Phase 1.

6.1. Modal results

First, modal analyses were conducted on three models. Note that due to nonlinear behavior, Nonlinear model failed to conduct modal analysis. Table 4 shows the first two normal mode shapes and natural
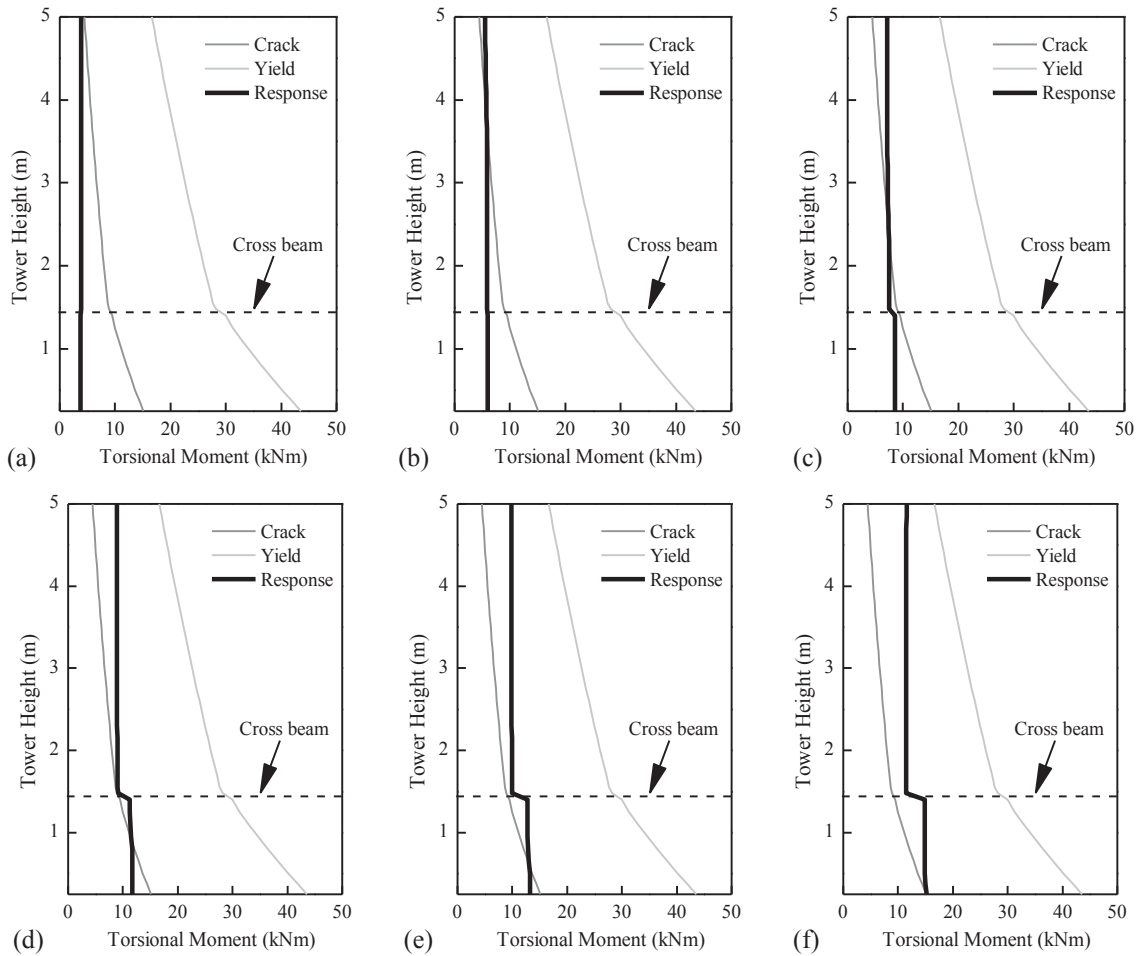
Fig. 15. Torsion moment of inclined tower leg: (a) 0.05 g, (b) 0.10 g, (c) 0.20 g, (d) 0.35 g, (e) 0.50 g and (f) 0.70 g.
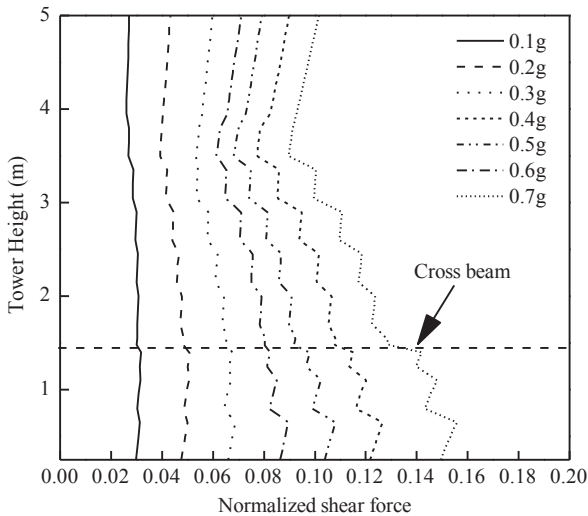

Fig. 16. Normalized shear force of inclined tower legs along tower height.

periods of two models using the initial stiffness of the bridge determined from the static equilibrium solution under dead loads. As the torsional stiffness of inclined tower legs decreased (from Elastic model to Crack model), periods of the first two modes slightly increased, reflecting increasing flexibility of the bridge in the longitudinal direction. This indicated that torsional stiffness to some extent contributed to the longitudinal vibration of the bridge and consequently seismic response

of the bridge.

6.2. Dynamic analysis results

The above three models are excited by earthquake waves within the tests. The following four different component responses are monitored and recorded: (1) maximum longitudinal displacement at tower top (DT); (2) maximum longitudinal displacement at deck end (DD); (3) maximum bending curvature at the crossbeam of inclined tower legs (CT) and (4) maximum cable force of C3 (FC). The discrepancy of maximum response of Elastic model and Crack model with respect to Nonlinear model is defined as:

$$\beta_i = \frac{R_i - R_{non}}{R_{non}} \tag{13}$$

where R_i is response of i model and i = Elastic model or crack model; R_{non} is the response of Nonlinear model. A positive value of β means overestimation of the seismic response while a negative value indicates underestimation. Fig. 19 shows the values of β for Elastic model and Crack model with respect to Nonlinear model.

For Elastic model, DT and DC will be slightly underestimated and the underestimation increases with the PGA. The maximum difference is around 7% and 5% for DT and DD respectively when PGA = 0.7 g. Meanwhile, before yielding of the tower leg (PGA < 0.3 g), CT is slightly overestimated about 4%, but tends to be underestimated after yielding (PGA > 0.3 g). The maximum underestimation of CT is approximately 8% when PGA = 0.7 g. Contrary to Elastic model, DT and DD of Crack mode will be overestimated for all the PGAs, and CT is underestimated before yielding of the tower leg but overestimated after
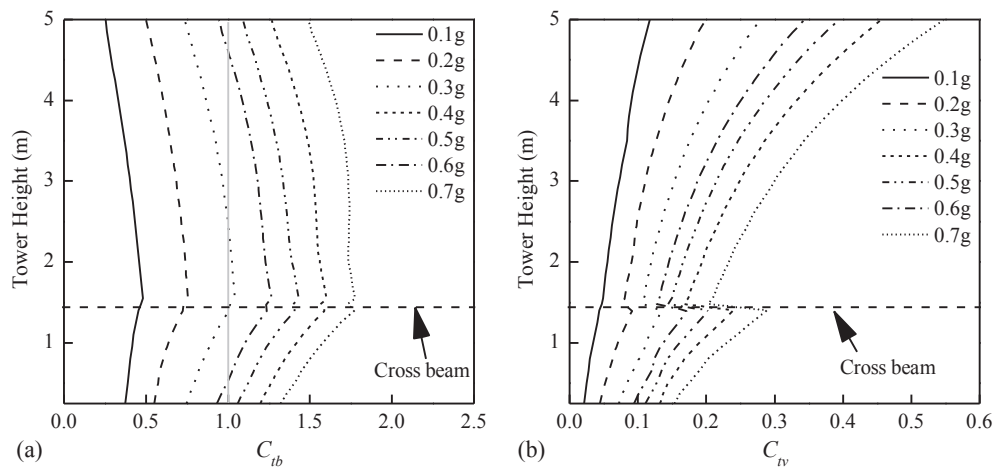
Fig. 17. Variation of C_{tb} and C_{tv} along tower height for different PGAs: (a) C_{tb} and (b) C_{tv}.
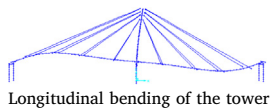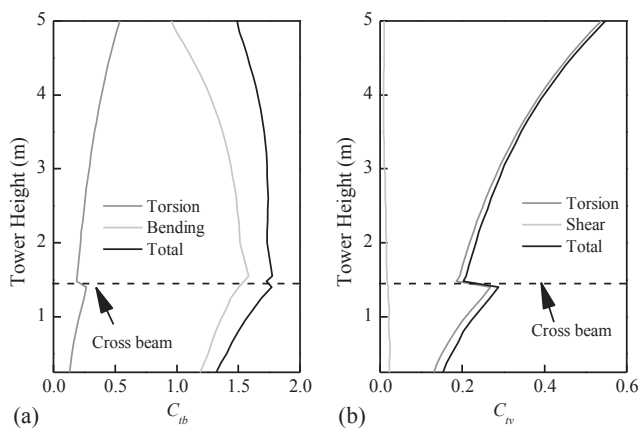

Fig. 18. Contribution of torsion, bending and shear to C_{tb} and C_{tv} at PGA = 0.7 g: (a) torsion and bending C_{tb}, and (b) torsion and shear C_{tv}.

Table 4
Modal shape and periods of three models.

Mode no.	Modal shape and description	Periods (s)	
Mode 1	Longitudinal sliding of the deck	Elastic model	1.149
		Nonlinear model	–
		Crack model	1.154
Mode 2	Longitudinal bending of the tower	Elastic model	0.545
		Nonlinear model	–
		Crack model	0.547

yielding. The maximum difference between Nonlinear model and Crack model is within 5% for all cases. For FC, both Elastic model and Crack model yield almost the same results as Nonlinear model, with the maximum difference less than 2%.

Taking the intersection (Section E-E) as an example, Table 5 lists the torsion moment for three models. For Elastic model, the torsional moment is the same as Nonlinear model before reaching crack torsion (PGA = 0.05 g). After that, the torsional moment of Elastic model increased steadily, and exceeded the yield moment (16.64 kN m) even at PGA = 0.15 g. Comparing to Elastic model, Nonlinear model considered substantial reduction of torsional stiffness of tower legs after crack torsion. This reduction helped alleviate the demand of tower torsional moment, which in turn delayed the torsional failure of the

tower legs. For Crack model, on the contrary, the torsional moment is largely underestimated comparing to Nonlinear model. The crack torsional moment is not exceeded until PGA = 0.7 g. Therefore, traditional approach which adopts a constant torsional stiffness (either using stiffness prior to or after crack torsional moment of the tower legs) will result in unrealistic torsional response.

7. Conclusion

To investigate earthquake-induced torsional response of a cable-stayed bridge with inclined tower legs, this paper conducted shake table tests on a 1/20 scaled cable-stayed bridge model. A description of the model design was presented and a numerical model which considered the reduction of torsional stiffness of inclined tower leg was established. The feasibility of numerical model was verified through a comparison of measured and numerical results. Further discussion was performed on different strategies to consider torsional stiffness of inclined tower leg and consequent seismic performance of the bridge. Conclusions were drawn from the current works as follows:

(1) During an earthquake, the bottom and middle region of inclined tower legs exhibited predominant flexural damage mode, while the region near the intersection suffered from a combination of flexural and torsional damage.
(2) With the reduction of torsional stiffness of inclined tower leg considered, the numerical model showed correlated results with the test model in displacement at tower top and deck end and cable force. The numerical model also predicted the flexural and torsional damage of inclined tower legs of the test model.
(3) Numerical results revealed that torsional crack moment can be easily reached at small PGAs, leading to substantial reduction of torsional stiffness of tower legs. This reduction helped to alleviate the demand of tower torsional moment, which in turn delayed the torsional failure of the tower legs.
(4) Based on numerical result, bending moment was the primary factor that caused concrete cracks at the lower inclined tower legs (Height < 4 m) whereas the contribution of torsion increased significantly at higher region of inclined tower legs (Height = 4–5 m), and the complex interaction of large bending moment and torsion resulted in flexural and torsional damage near the intersection. On the other hand, shear force made a negligible contribution to the damage of inclined tower legs.
(5) Conventional ways, which adopt an elastic behavior of torsion either with stiffness prior to or after crack torsional moment, will lead to slight errors in predicting displacement response at tower top and deck end, cable force and bending response of the tower, and
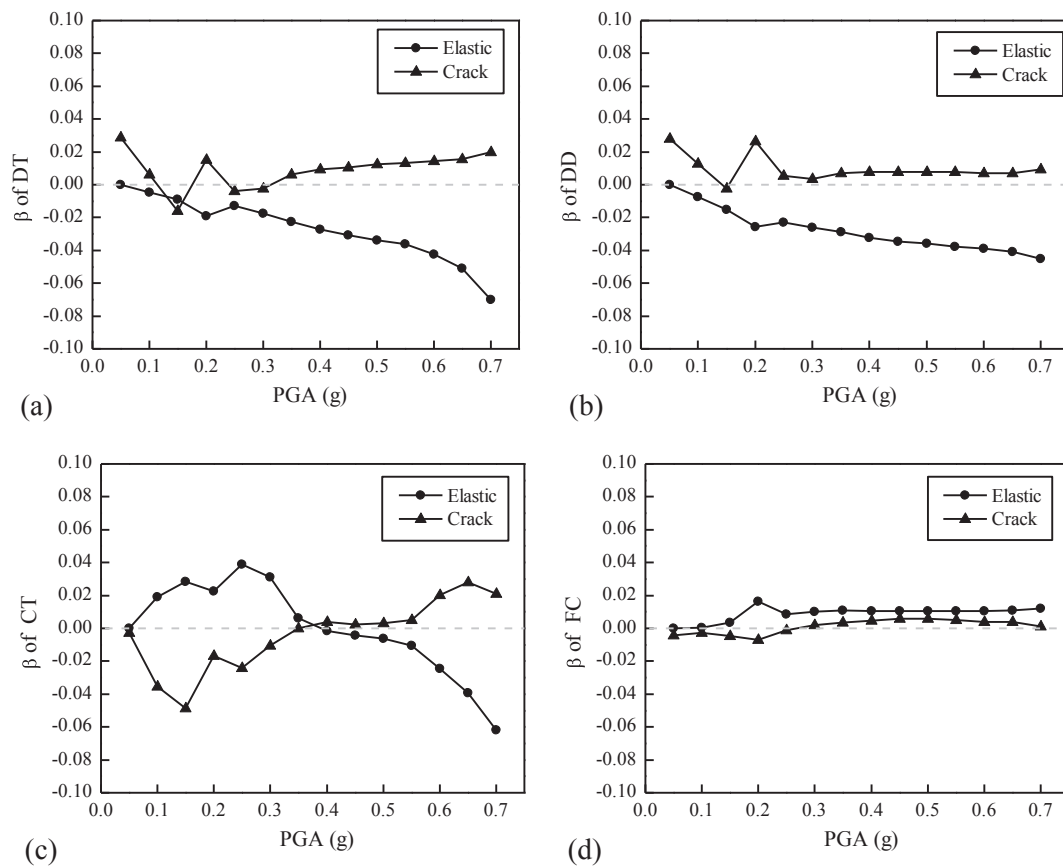
Fig. 19. Discrepancy of the maximum response (β) of Elastic model and Crack model with respect to Nonlinear model for: (a) DT, (b) DC, (c) CT and (d) FC.

Table 5
Torsion moment of intersection for three models (Unit: kN m).

PGA(g)	0.05	0.10	0.15	0.20	0.25	0.30	0.35	0.40	0.45	0.50	0.55	0.60	0.65	0.70
Elastic model	4.3	9.3	17.3	20.5	28.0	33.1	38.4	42.7	46.6	49.8	52.9	57.8	61.5	66.4
Nonlinear model	4.3	5.7	7.0	7.4	8.2	8.7	9.3	9.7	10.1	10.4	10.7	11.1	11.6	12.2
Crack model	0.4	0.8	1.5	1.8	2.4	2.9	3.4	3.8	4.2	4.5	4.8	5.2	5.7	6.3

result in intensive overestimation or underestimation of torsional response of the inclined tower legs.

Acknowledgements

Appendix A. Supplementary material

Supplementary data to this article can be found online at https://doi.org/10.1016/j.engstruct.2018.12.081.

References

[1] Calvi GM, Sullivan TJ, Villani A. Conceptual seismic design of cable-stayed bridges. J Earthq Eng 2010;14(8):1139–71.
[2] Wang RL. Experimental and method research on transverse seismic mitigation of medium span cable-stayed bridges [Ph.D. thesis]. Shanghai, China: Tongji University; 2016.
[3] Ali HEM, Abdel-Ghaffar AM. Seismic passive control of cable-stayed bridges. Shock Vib 1995;2(4):259–72.
[4] Abdel-Ghaffar AM, Aly SN. 3-D nonlinear seismic behavior of cable-stayed bridges. J Struct Eng 1997;117(11):3456–76.
[5] Ren WX, Makoto O. Elastic-plastic seismic behavior of long span cable-stayed bridges. J Bridge Eng 1999;4(3):194–203.

[6] Wilson JC, Wayne G. Modelling of a cable-stayed bridge for dynamic analysis. Earthq Eng Struct Dyn 1991;20(8):707–21.
[7] Prakash S, Belarbi A, You YM. Seismic performance of circular RC columns subjected to axial force, bending, and torsion with low and moderate shear. Eng Struct 2010;32(1):46–59.
[8] Hsu TTC. Torsion of reinforced concrete. New York: Van Nostrand Reinhold; 1984.
[9] Elnashai AS, Di SL. Fundamentals of earthquake engineering. New York: John Wiley & Sons; 2008.
[10] Rahal KN, Michael PC. Compatibility torsion in spandrel beams using modified compression field theory. ACI Mat J 2006;103(3):328.
[11] Modena C, Tecchio G, Pellegrino C, et al. Reinforced concrete and masonry arch bridges in seismic areas: typical deficiencies and retrofitting strategies. Struct Infr Eng 2015;11(4):415–42.
[12] ACI Committee 318. Building code requirements for structural concrete (ACI318-08) and commentary (ACI 318R-08). Farmington (MI): American Concrete Institute; 2008.
[13] American Association of State Highway and Transportation Officials (AASHTO). AASHTO LRFD bridge design specifications. 5th ed. Washington, DC: AASHTO; 2012.
[14] Ok SY, Kim DS, Park KS, et al. Semi-active fuzzy control of cable-stayed bridges using magneto-rheological dampers. Eng struct 2007;29(5):776–88.
[15] Chang KC, Mo YL, Chen CC, et al. Lessons learned from the damaged Chi-Lu cable-stayed bridge. J Bridge Eng 2004;9(4):343–52.
[16] Siringoringo DM, Fujino Y, Namikawa K. Seismic response analyses of the Yokohama Bay cable-stayed bridge in the 2011 great East Japan Earthquake. J Bridge Eng 2013;19(8):A4014006.
[17] Park RL, Park R, Paulay T. Reinforced concrete structures. New York: John Wiley & Sons; 1975.
[18] Pellegrino C, Zanini MA, Zampieri P, et al. Contribution of in situ and laboratory investigations for assessing seismic vulnerability of existing bridges. Struct Infr Eng 2015;11(9):1147–62.

[19] Rahal KL, Collins MP. Analysis of sections subjected to combined shear and torsion-a theoretical model. ACI Struct J 1995;92:459.

[20] Lampert P. Post-cracking stiffness of reinforced concrete beams in torsion and bending. ACI Special Publication; ACI 1973;SP-35:385–433.

[21] Yi J, Li J. Longitudinal seismic behavior of a single-tower cable-stayed bridge subjected to near-field earthquakes. Shock Vib 2017;2017:1675982.

[22] Nazmy AS, Abdel-Ghaffar AM. Non-linear earthquake response analysis of long-span cable-stayed bridges: theory. Earthq Eng Struct Dyn 1990;19(1):45–62.

[23] Bernardo LF, Lopes SM. Behaviour of concrete beams under torsion: NSC plain and hollow beams. Mat Struct 2008;41(6):1143–67.

[24] Markeset G, Hillerborg A. Softening of concrete in compression—localization and size effects. Cem Concr Res 1995;25(4):702–8.

[25] McKenna F. OpenSees: a framework for earthquake engineering simulation. Comput Sci Eng 2011;13(4):58–66.

[26] Rajeev P, Tesfamariam S. Seismic fragilities for reinforced concrete buildings with consideration of irregularities. Struct Saf 2012;39:1–13.

[27] Sepe V, Spacone E, Raka E, et al. Seismic analysis of masonry buildings: equivalent frame approach with fiber beam elements. In Cunha A, Caetano E, Ribeiro P, Müller G. Proceedings of the 9th international conference on structural dynamics EURODYN 2014. p. 237–44.

[28] Kent DC, Park R. Flexural members with confined concrete. J Struct Div 1971;97(7):1969–90.

[29] Pan Z, Li B, Lu Z. Effective shear stiffness of diagonally cracked reinforced concrete beams. Eng Struct 2014;59:95–103.

[30] Priestley MJN, Seible F, Calvi GMS. Seismic design and retrofit of bridges. New York: John Wiley & Sons; 1996.

[31] Ernst JH. Der E-Modul von Seilen unter berucksichtigung des Durchhanges. Der Bauingenieur 1965;40(2):52–5. [in German].

[32] Xiang N, Li J. Experimental and numerical study on seismic sliding mechanism of laminated-rubber bearings. Eng Struct 2017;141:159–74.

[33] Choi E, DesRoches R, Nielson B. Seismic fragility of typical bridges in moderate seismic zones. Eng Struct 2004;26(2):187–99.

[34] American Association of State Highway and Transportation Officials (AASHTO). AASHTO guide specifications for LRFD seismic bridge design. Washington, DC: AASHTO; 2011.

[35] Kemp EL, Sozen MA, Siess CP. Torsion in reinforced concrete. University of Illinois at Urbana-Champaign; 1961; research series NO.226.

[36] Mondal TG, Prakash SS. Nonlinear finite-element analysis of RC bridge columns under torsion with and without axial compression. J Bridge Eng 2015;21(2):04015037.

[37] Gregori JN, Sosa PM, Prada MF, et al. A 3D numerical model for reinforced and prestressed concrete elements subjected to combined axial, bending, shear and torsion loading. Eng Struct 2007;29(12):3404–19.

[38] Greene JG, Belarbi A. Model for reinforced concrete members under torsion, bending, and shear. I: Theory. J Eng Mech 2009;135(9):961–9.

[39] Greene JG, Belarbi A. Model for reinforced concrete members under torsion, bending, and shear. II: Model application and validation. J Eng Mech 2009;135(9):970–7.

[40] Benavent-Climent A, Cahís X, Vico JM. Interior wide beam-column connections in existing RC frames subjected to lateral earthquake loading. Bull Earthq Eng 2010;8(2):401–20.

[41] Rahal KL, Collins MP. Analysis of sections subjected to combined shear and torsion-a theoretical model. ACI Struct J 1995;92(4):459.

[42] Lampert P, Collins MP. Torsion, bending, and confusion—an attempt to establish the facts. ACI J Proc 1972;69(8):500–4.

[43] Ersoy U, Ferguson PM. Concrete beams subjected to combined torsion and shear-experimental trends. ACI Spec Publ 1968;18(1):441–60.